Journal of Alloys and Compounds 486 (2009) 738–742

Contents lists available at ScienceDirect

Journal of Alloys and Compounds

journal homepage: www.elsevier.com/locate/jallcom

Effect of anodic dissolution in multi-element nanoparticles on methanol electro-oxidation

Yi-Fan Hsieh, Kung-Yu Yeh, Pu-Wei Wu*, Yu-Chi Hsieh, Pang Lin

Department of Materials Science and Engineering, National Chiao Tung University, 1001 Ta Hsueh Road, Hsin-Chu 30010, Taiwan, ROC

ARTICLE INFO

Article history:
Received 6 March 2009
Received in revised form 6 July 2009
Accepted 7 July 2009
Available online 16 July 2009

Keywords:
Electrode materials
Metals
Electrochemical reactions

ABSTRACT

Radio frequency sputter deposition was used to deposit multi-element nanoparticles on carbon clothes for methanol electro-oxidation. Results from energy dispersive spectroscope confirmed the composition was $Pt_{35}Fe_{12}Co_{12}Ni_{20}Cu_{12}Ag_9$. X-ray diffraction pattern suggested a fcc phase. An electrochemical de-alloying treatment was conducted in an acidic electrolyte with multiple potential sweeps at a scan rate of 20 mV/s for 0–0.3, 0–0.5, and 0–0.7 V, respectively. Images from scanning electron microscope after anodic dissolutions demonstrated considerable variations in surface morphologies. Measurements on hydrogen desorption also revealed substantial increase in electrochemical active surface area. Current responses from cyclic voltammetry indicated the sample of 0–0.5 V anodic dissolution with notable enhancement. In mass activities, the same sample exhibited a comparable value to that of $Pt_{43}Ru_{57}$.

1. Introduction

Materials to promote methanol electro-oxidations have been investigated intensively in the past decades because their developments are critical for direct methanol fuel cells (DMFCs) [1,2]. Since electrolytes in DMFCs are corrosive in nature, conventional candidates for electrocatalysis are noble metals or oxides because their recognized chemical stabilities ensure reasonable lifetime [3–5]. Among them, the Pt and alloys of Pt have received considerable attentions, as evidenced by extensive reports covering a variety of compositions and morphologies with impressive electrochemical behaviors [6–8]. In general, the electro-oxidation of methanol involves successive de-hydrogenation steps, leaving CO chemically bond to the Pt surface. Therefore, secondary elements responsible for oxidizing the adsorbed CO are necessary. Currently, it is established that Ru is effective in removing the CO, and nanoparticles of PtRu reveal the highest catalytic ability for methanol electro-oxidations [9,10]. Unfortunately, due to excessive cost for Pt and Ru, search of less expensive elements with comparable performances is still in pursuit.

The simplest way to improve catalytic performances is to increase the catalyst loading. However, this approach often leads to undesirable material costs. An alternative route is to synthesize electrocatalysts with large active areas. One of the methods under studies is the electrochemical de-alloying process in which elements with relatively more positive redox potentials are electrochemically removed under deliberate anodic polarizations, leaving elements with less positive redox potentials mostly intact [11,12]. For example, Liu et al. electrodeposited a PtCu film and dissolved the Cu potentiostatically at 0.35 V, rendering a nanoporous Pt film with significantly enhanced surface area [13]. A similar process is adopted by Koh and Strasser where nanoparticles of $Pt_{25}Cu_{75}$ were converted to $Pt_{79}Cu_{21}$ by repeated cyclic voltammetric scans in an acidic electrolyte [14]. Substantial activity enhancements for the oxygen reduction reaction were observed, which are attributed to a favorable structural arrangement of Pt atoms at the particle surface.

The de-alloying process becomes rather complicated once nanoparticles contain three or more elements. It is because their redox potentials vary, and distinct morphologies and compositions are possible contingent on the anodizing potentials imposed. For instance, Srivastava et al. developed a three-step procedure to de-alloy Cu from nanoparticulate PtCoCu, and reported impressive oxygen reduction behaviors [15]. Formation of metals with multiple principal elements was first demonstrated by Yeh et al. with the objective to develop high-entropy alloys [16]. On the other hand, the synthesis of multi-element nanoparticles has received less attention. Recently, in our group we employed a radio frequency sputter deposition to prepare multi-element nanoparticles (PtFeCoNiCuAg) in various compositions, and studied their catalytic abilities on methanol electro-oxidations [17,18]. We realize that due to substantial difference in their redox potentials, further improvements in electrocatalysis are likely if the de-alloyed process is properly carried out.

In this work, we fabricated multi-element nanoparticles and conducted de-alloying treatments at various potentials to enhance active surface areas for methanol electro-oxidation.

* Corresponding author. Tel.: +886 3 5131227; fax: +886 3 5724727.
E-mail address: ppwu@mail.nctu.edu.tw (P.-W. Wu).

0925-8388/$ – see front matter © 2009 Elsevier B.V. All rights reserved.
doi:10.1016/j.jallcom.2009.07.055

2. Experimental

2.1. Deposition of the multi-element nanoparticles

Multi-element nanoparticles were deposited on carbon clothes (E-TEK) using a radio frequency sputter. The as-received carbon cloth was coated with carbon slurry composed of 70 wt% Shawinigan Acetylene Black (Chevron) and 30 wt% polytetrafluoroethylene (Dupont) to reach a total dry weight of 22 mg/cm^2. To prepare sputter target, metallic powders including Fe (10.3 μm), Co (1.4 μm), Ni (2.5 μm), Cu (45.0 μm), and Ag (0.8 μm) were mixed at a molar ratio of 24:22:21:15:18. After dry tumbling for 24 h under N_2, the mixture underwent a hydraulic pressing at 2500 psi for 30 s to make a disk with 3.0 in. in diameter. Next, Pt foils (99.9 wt%, 1 cm × 1 cm) were positioned atop the disk to add the Pt atoms into the sputtered flux. The size for the carbon cloth was 4 cm × 4 cm, and the sputter deposition lasted 5 min. The carbon cloth underwent a rotating motion to obtain uniform coverage during sputter deposition. Details processing steps and a schematic for the experimental setup were reported previously [17].

2.2. Materials characterizations for the multi-element nanoparticles

Identification for relevant phase present in the as-prepared multi-element film was conducted by a XRD with Cu Kα radiation (λ = 1.5418 Å) (Siemens D5000). The specimen was subjected to a sputter deposition for 120 min to ensure sufficient loading. SEM (JSM-6500F) was used to observe morphologies of the multi-element nanoparticles before and after anodic dissolutions. An energy dispersive X-ray spectroscope (EDX) was employed to obtain the molar ratio for the multi-element nanoparticles. In mass activity determination, an inductively coupled plasma mass spectrometry (ICP-MS; SCIEX ELAN 5000) was adopted where the samples were dissolved in a solution containing HCl, HNO_3, and HF at a 2:2:1 volume ratio.

2.3. Anodic dissolutions and electrochemical analysis

Electrochemical characterizations were performed using a Solartron SI 1287 at 26 °C in a three-electrode configuration in which a Pt foil (8 cm^2) and Ag/AgCl were used as counter and reference electrodes, respectively. The area for the working electrode was 1 cm^2. Anodic dissolutions for the multi-element nanoparticles were carried out in 1 M H_2SO_4 aqueous solution in linear voltage sweeps for 100 cycles at a scan rate of 20 mV/s. The voltage ranges selected were 0–0.3, 0–0.5, and 0–0.7 V. Upon completion, the samples were immersed in an aqueous solution consisted of 0.5 M H_2SO_4 and 1 M CH_3OH to study their catalytic abilities on the methanol electrooxidation. Before measurements, the electrolyte was purged with N_2 for 15 min and waited for 30 min to stabilize the open circuit voltage. Then, cyclic voltammetry (CV) was adopted in a voltage range of 0–0.95 V at a scan rate 50 mV/s. In addition, we obtained the values for electrochemically active surface area (ESA) by conducting hydrogen desorption analysis. The ESA was obtained by a CV scan for a voltage range of −0.2 to 1.0 V in a 0.5 M H_2SO_4 aqueous solution at a scan rate of 10 mV/s.

3. Results and discussion

3.1. Characterizations of multi-element nanoparticles

Since the sputtering yield varies considerably in each element, the atomic ratio for the multi-element nanoparticles can only be determined empirically. Results from multiple EDX analysis on relatively large area SEM samples confirmed the composition was $Pt_{35}Fe_{12}Co_{12}Ni_{20}Cu_{12}Ag_9$. We realized that the sputter deposition technique might produce minute local variation in the deposit composition. But the EDX provided the statistical average for the as-prepared samples so the composition of $Pt_{35}Fe_{12}Co_{12}Ni_{20}Cu_{12}Ag_9$ should be reliable. The XRD pattern on the multi-element nanoparticles after 120 min of sputter deposition is demonstrated in Fig. 1. Due to interference from the carbon cloth, the diffraction pattern contained moderate noises. Nevertheless, we were able to identify diffraction signals from Pt, C, and polytetrafluoroethylene (PTFE). Notably, the Pt existed in a fcc lattice with relative intensity in proper order. The positions for the Pt (1 1 1), Pt (2 0 0), Pt (2 2 0), and Pt (3 1 1) were located at 39.8°, 46.2°, 67.5°, and 81.3°, respectively. These angles were slightly shifted as opposed to the unalloyed Pt lattice. Since the atomic ratio for Fe, Co, Ni, and Cu are smaller than that of Pt, the resulting lattice parameter for the multi-element nanoparticles was reduced as expected following Vegard's law.

Fig. 2 exhibits the SEM images for the carbon cloth and as-prepared multi-element nanoparticles. As shown in Fig. 2(a), the carbon cloth was decorated with carbon particles in irregular shape,

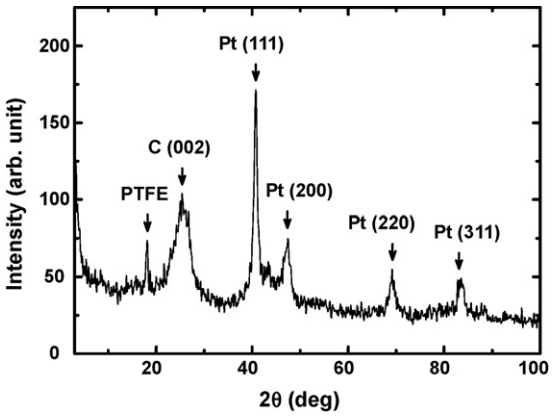

Fig. 1. X-ray diffraction pattern for the multi-element nanoparticles after 120 min of sputter deposition.

and their average size was approximately 40 nm. After deposition for 5 min, as shown in Fig. 2(b), there appeared surface nodules on individual carbon particles and the average particle size was increased to 80 nm. The sputter rate for the multi-element nanoparticles was estimated at 4 nm/min.

3.2. Effects of anodic dissolutions

Anodic dissolutions conducted in various voltage regimes are expected to produce distinct de-alloying behaviors because the redox potentials for individual elements differ considerably. In an acidic electrolyte, elements with a positive redox potential are

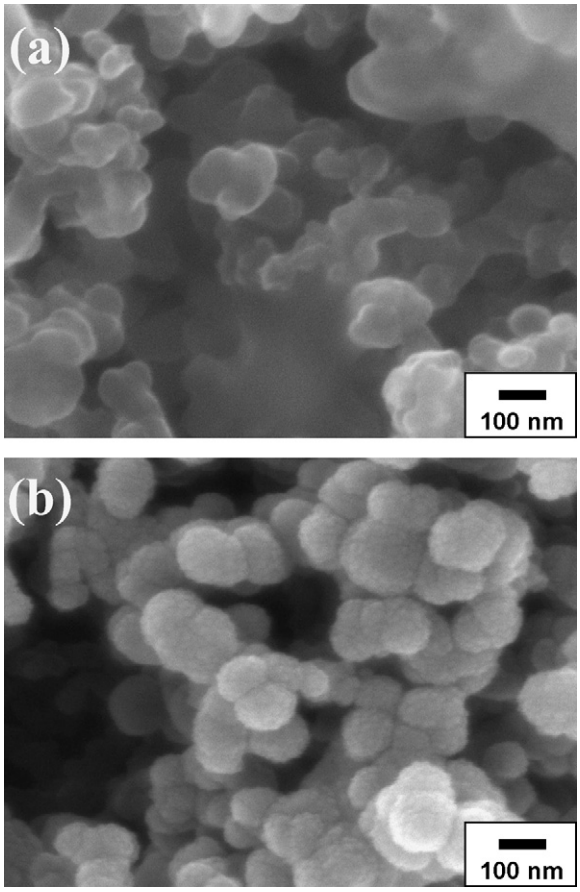

Fig. 2. SEM images for the carbon cloth (a) before sputter deposition, and (b) 5 min of sputter deposition.

Table 1
Values for standard redox potentials for Pt, Fe, Co, Ni, Cu, and Ag. The H_2/H^+ represents 0 V.

Reaction	E^0 (V)
$Pt_{(s)} \rightarrow Pt^{2+}_{(aq)} + 2e$	−1.20
$Ag_{(s)} \rightarrow Ag^{+}_{(aq)} + e$	−0.80
$Cu_{(s)} \rightarrow Cu^{2+}_{(aq)} + 2e$	−0.34
$H_{2(g)} \rightarrow 2H^{+}_{(aq)} + 2e$	0.00
$Ni_{(s)} \rightarrow Ni^{2+}_{(aq)} + 2e$	0.25
$Co_{(s)} \rightarrow Co^{2+}_{(aq)} + 2e$	0.28
$Fe_{(s)} \rightarrow Fe^{2+}_{(aq)} + 2e$	0.44

susceptible to spontaneous dissolutions without external stimuli. The tendency for dissolution becomes more pronounced when the redox potential becomes more positive. On the other hand, elements with a negative one infer chemical stability unless the anodizing voltage sufficiently compensates the negative redox value. Table 1 lists the redox potentials for the Pt, Fe, Co, Ni, Cu, Ag, and H_2. Among the elements present, the order for anodic dissolutions is Fe, Co, Ni, Cu, Ag, and Pt. Since we performed the anodic dissolution in multiple linear sweeps, a larger voltage sweep not only suggested stronger anodizing power but also indicated longer immersion time in the electrolyte.

The compositions for the multi-element nanoparticles after anodic dissolutions are provided in Table 2. Notably, all samples became Pt-rich. For samples undergoing anodic dissolution in 0–0.3 V, we observed complete loss of Fe and Co, with the resulting composition confirmed as $Pt_{48}Ni_{18}Cu_{17}Ag_{17}$. For samples experiencing anodic dissolution in 0–0.5 V, additional Cu and Ag were dissolved and the composition was $Pt_{86}Ni_{14}$. Further anodization for samples in 0–0.7 V resulted in more Ni loss as the composition became $Pt_{89}Ni_{11}$. The presence of Ni after anodic dissolutions was likely due to its preponderance in the as-deposited state.

Fig. 3 demonstrates the SEM images for the multi-element nanoparticles after anodic dissolutions of 0–0.3, 0–0.5, and 0–0.7 V, respectively. Apparently, the size for the multi-element nanoparticles became smaller when the anodic voltage was increased. For the voltage ranges in 0–0.3 and 0–0.5 V, the particle size was reduced to 70 and 60 nm, respectively. Interestingly, distinct morphological changes were observed when the anodizing voltage was raised to 0.7 V where the as-prepared nodular structure was transformed to textural surface with moderate coalescences. However, the exact nature for this phenomenon is still unclear.

Electrodes with altered morphologies often can be confirmed by ESA measurements. Fig. 4 exhibits the ESA curves for the as-prepared nanoparticles and samples after anodic dissolutions. According to Navessin et al. and Liu et al., appearance of anodic and cathodic spikes in −0.2 to 0 V are attributed to desorption and absorption of hydrogen [19,20]. Since the hydrogen desorption takes place exclusively on surface Pt sites, the ESA of Pt is estimated by integrating the coulombic charge in the desorption regime. The as-prepared multi-element nanoparticles revealed a ESA of 15.5 cm^2. Remarkably, once anodic dissolutions were performed, the resulting ESA was increased significantly. Their values were 26.1, 36, and 34.2 cm^2 for samples undergoing 0–0.3, 0–0.5, and 0–0.7 V treatments. Despite the notable difference in surface morphologies, the ESA from anodization of 0–0.7 V was similar

Table 2
Compositions from EDS in molar ratios for multi-element nanoparticles with and without anodic dissolutions.

	Pt	Fe	Co	Ni	Cu	Ag	Total (%)
As-prepared	35	12	12	20	12	9	100
0–0.3 V	48	0	0	18	17	17	100
0–0.5 V	86	0	0	14	0	0	100
0–0.7 V	89	0	0	11	0	0	100

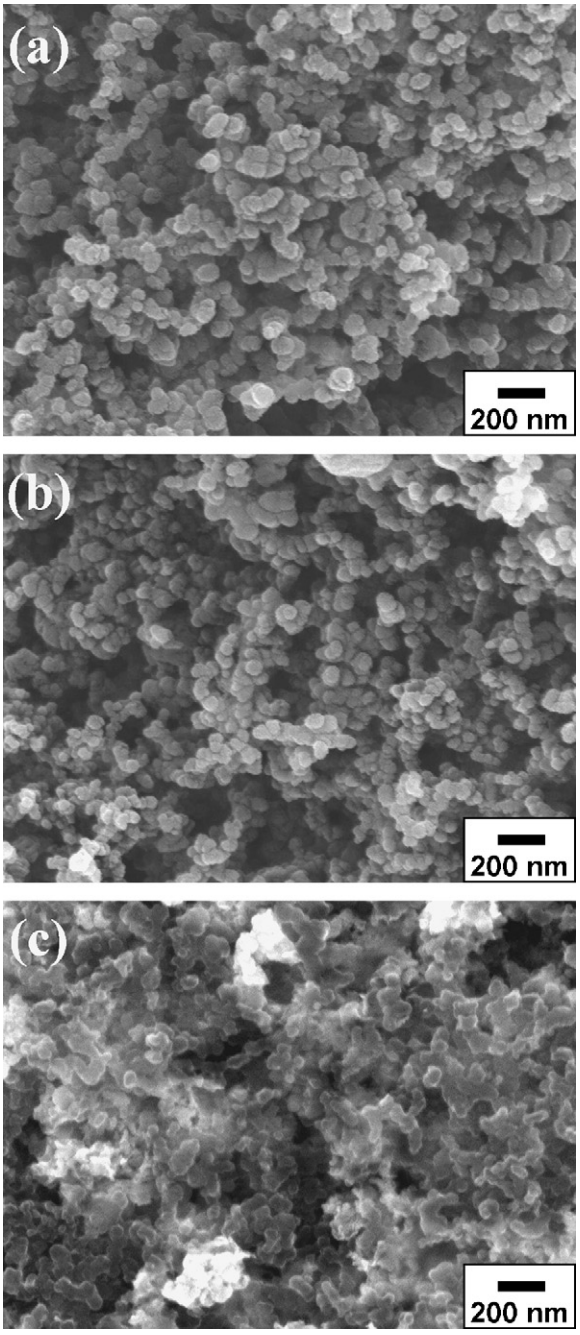

Fig. 3. SEM images for the $Pt_{35}Fe_{12}Co_{12}Ni_{20}Cu_{12}Ag_9$ after anodic dissolutions in (a) 0–0.3, (b) 0–0.5, and (c) 0–0.7 V, respectively.

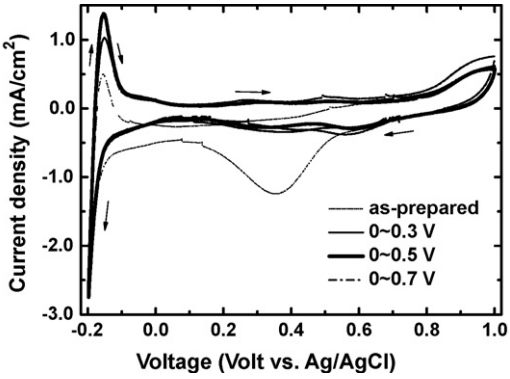

Fig. 4. CV curves for the hydrogen adsorption and desorption.

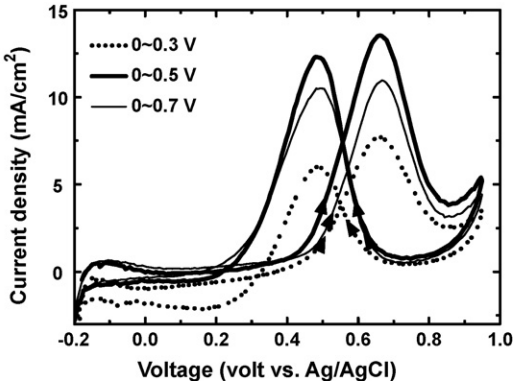

Fig. 5. CV curves in apparent current densities for the $Pt_{35}Fe_{12}Co_{12}Ni_{20}Cu_{12}Ag_9$ after anodic dissolutions of 0–0.3, 0–0.5, and 0–0.7 V, respectively.

to that of 0–0.5 V. This indicated anodic dissolution conducted at 0–0.5 V is adequate for ESA enhancement without unnecessary material loss.

3.3. Characterizations on methanol electro-oxidation

Fig. 5 presents the CV profiles for the multi-element nanoparticles after anodic dissolutions of 0–0.3, 0–0.5, and 0–0.7 V, respectively. In each sample, there appeared current responses during forward and backward scans. According to literature, currents from the forward scan are due to the oxidation of methanol while those of backward scan are attributed to the oxidation of carbonaceous species produced from the forward scan [21]. The peak current densities during forward and backward scans are defined as i_f and i_b. Its ratio, i_f/i_b, indicates the catalytic ability to remove CO [22]. As shown in the CV profiles, the sample undergoing 0–0.5 V anodic dissolution revealed the highest current responses. In contrast, the one with 0–0.3 V showed the lowest one. Their i_f/i_b ratios were between 1.10 and 1.29, which is consistent with what was reported earlier on Pt-based electrocatalysts [23].

Because anodic dissolutions inevitably resulted in weight loss, true catalytic abilities can only be evaluated by determining their mass activities (mA/mg). For this purpose, we also conducted similar sputter depositions to prepare Pt and $Pt_{43}Ru_{57}$-catalyzed carbon clothes. Fig. 6 provides the CV profiles in mass activities for the multi-element nanoparticles in as-prepared state and after anodic dissolution of 0–0.5 V. The curves of Pt and $Pt_{43}Ru_{57}$ were also shown here for comparison purpose [18]. Relevant electrochemical parameters are listed in Table 3. Among them, the $Pt_{43}Ru_{57}$ exhibited the highest mass activity with a i_f/i_b ratio of 1.57. These behaviors confirmed the superiority of PtRu as an effective catalyst

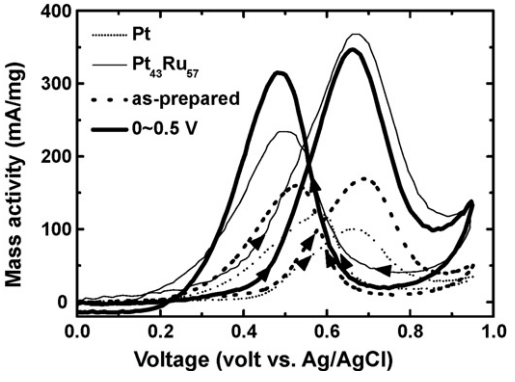

Fig. 6. CV curves in mass activities for the $Pt_{35}Fe_{12}Co_{12}Ni_{20}Cu_{12}Ag_9$ in as-prepared state, and anodic dissolution of 0–0.5 V, as well as Pt and $Pt_{43}Ru_{57}$.

Table 3
Electrochemical parameters from the CV scans in mass activities.

	Pt loading (mg)	Forward		Backward		i_f/i_b
		V_f[a] (mV)	i_f[b] (mA/Pt mg)	V_b[c] (mV)	i_b[d] (mA/Pt mg)	
As-prepared	0.11	0.69	168.57	0.53	160.29	1.05
0–0.5 V	0.04	0.66	346.92	0.48	315.38	1.10
Pt	0.16	0.66	100.32	0.59	122.13	0.82
$Pt_{43}Ru_{57}$	0.07	0.67	368.00	0.50	234.00	1.56

[a] Peak potential in forward scan.
[b] Peak mass activity in forward scan.
[c] Peak potential in backward scan.
[d] Peak mass activity in backward scan.

for methanol electro-oxidation, a fact well-established in literature. Interestingly, the sample after anodic dissolution of 0–0.5 V exhibited a comparable anodic mass activity. However, its i_f/i_b ratio was still inferior to that of $Pt_{43}Ru_{57}$. On the other hand, samples of as-prepared multi-element nanoparticles and Pt demonstrated reduced catalytic behaviors in both mass activities and i_f/i_b ratios. These results clearly demonstrate the positive effects of anodic dissolutions in enhancing the catalytic abilities of multi-element nanoparticles.

4. Conclusions

Sputter deposition was employed to prepare multi-element nanoparticles for methanol electro-oxidation. EDS determined the composition as $Pt_{35}Fe_{12}Co_{12}Ni_{20}Cu_{12}Ag_9$ and XRD pattern indicated a fcc phase. Electrochemical de-alloying process was performed by multiple voltage sweeps in an acidic electrolyte at potentials of 0–0.3, 0–0.5, and 0–0.7 V. After anodic dissolutions, the surface morphologies were altered with substantial increase in ESA. In mass activities, the sample after 0–0.5 V anodic dissolution revealed a comparable mass activity to that of $Pt_{43}Ru_{57}$, albeit with a lower i_f/i_b. Nevertheless, its catalytic abilities were improved significantly over those of as-prepared multi-element nanoparticles and Pt.

Acknowledgements

The authors would like to express their gratitude to Professor Chiun-Hsun Chen of Mechanical Engineering Department for equipment supports. Discussions over multi-element alloy formations with Professor Cheun-Guang Chao of Materials Science and Engineering Department is appreciated.

References

[1] B.C.H. Steele, A. Heinzel, Nature 414 (2001) 345.
[2] Z.B. Wang, G.P. Yin, P.F. Shi, J. Alloys Compd. 420 (2006) 126.
[3] H.N. Dinh, X. Ren, F.H. Garzon, P. Zelenay, S. Gottesfeld, J. Electroanal. Chem. 491 (2000) 222.
[4] N. Ren, A.G. Dong, W.B. Cai, Y.H. Zhang, W.L. Yang, S.J. Huo, Y. Chen, S.H. Xie, Z. Gao, Y. Tang, J. Mater. Chem. 14 (2004) 3548.
[5] H.J. Ahn, J.S. Jang, Y.E. Sung, T.Y. Seong, J. Alloys Compd. 473 (2009) L28.
[6] H.J. Ahn, H.S. Shim, W.B. Kim, Y.E. Sung, T.Y. Seong, J. Alloys Compd. 471 (2009) L39.
[7] J.F. Whitacre, T. Valdez, S.R. Narayanan, J. Electrochem. Soc. 152 (2005) A1780.
[8] Y.J. Song, S.B. Han, J.M. Lee, K.W. Park, J. Alloys Compd. 473 (2009) 516.
[9] T. Yajima, H. Uchida, M. Watanabe, J. Phys. Chem. B 108 (2004) 2654.
[10] P. Waszczuk, G.Q. Lu, A. Wieckowski, C. Lu, C. Rice, R.I. Masel, Electrochim. Acta 47 (2002) 3637.
[11] J. Erlebacher, M.J. Aziz, A. Karma, N. Dimitrov, K. Sieradzki, Nature 410 (2001) 450.
[12] Z. Liu, S. Koh, C. Yu, P. Strasser, J. Electrochem. Soc. 154 (2007) B1192.
[13] H. Liu, P. He, Z. Li, J. Li, Nanotechnology 17 (2006) 2167.
[14] S. Koh, P. Strasser, J. Am. Chem. Soc. 129 (2007) 12624.
[15] R. Srivastava, P. Mani, N. Hahn, P. Strasser, Angew. Chem. Int. Ed. 46 (2007) 1.

[16] J.W. Yeh, S.K. Chen, S.J. Lin, J.Y. Gan, T.S. Chin, T.T. Shun, C.H. Tsau, S.Y. Chang, Adv. Eng. Mater. 6 (2004) 299.
[17] C.F. Tsai, P.W. Wu, P. Lin, C.G. Chao, K.Y. Yeh, Jpn. J. Appl. Phys. 47 (2008) 5755.
[18] C.F. Tsai, K.Y. Yeh, P.W. Wu, Y.F. Hsieh, P. Lin, J. Alloys Compd. 478 (2009) 868.
[19] T. Navessin, M. Eikerling, Q. Wang, D. Song, Z. Liu, J. Horsfall, K.V. Lovell, S. Holdcroft, J. Electrochem. Soc. 152 (2005) A796.
[20] Z. Liu, X.Y. Ling, B. Guo, L. Hong, J.Y. Lee, J. Power Sources 167 (2007) 272.
[21] Y.J. Gu, W.T. Wong, Langmuir 22 (2006) 11447.
[22] J. Bagchi, S.K. Bhattacharya, J. Power Sources 163 (2007) 661.
[23] W. Jingjie, T. Haolin, P. Mu, W. Zhaohui, M. Wentao, Electrochim. Acta 54 (2009) 1473.